Gamma-ray multiplicities in evaporation residues formed in bombardments of ^{150}Nd by ^{20}Ne‡

D. G. Sarantites
Department of Chemistry, Washington University, St. Louis, Missouri 63130

J. H. Barker
Department of Physics, St. Louis University, St. Louis, Missouri 63103

M. L. Halbert, D. C. Hensley, R. A. Dayras, E. Eichler,† and N. R. Johnson
Oak Ridge National Laboratory, Oak Ridge, Tennessee 37830*

S. A. Gronemeyer
Department of Physics, Washington University, St. Louis, Missouri 63130

(Received 28 June 1976)

The first three moments of the multiplicity distribution were deduced for the γ-ray cascades in the evaporation residues produced in bombardments of ^{150}Nd with ^{20}Ne at four energies from 127.7 to 172.4 MeV by means of measurements of the first and higher order coincidence rates between a Ge(Li) spectrometer and eight NaI(Tl) detectors. The cross sections for the production of $^{160-165}$Yb and $^{156-161}$Er were also measured. The average multiplicity $\langle M_J \rangle$ and the width of the multiplicity distribution σ_{M_J} for cascades via a state of spin J were found to be independent of J. For a given product, $\langle M \rangle$ and σ_M increase with bombardment energy but for fixed energy they decrease with increasing number of emitted neutrons. The observed values of $\langle M \rangle$ and σ_M range from 11 to 32 and 6 to 9, respectively. The multiplicities $\langle M \rangle$ in the (^{20}Ne, $xn\alpha$) products are considerably lower than those for (^{20}Ne, xn) but the widths σ_M are the same for a given value of x. The skewness of the multiplicity distribution is negative, approaching zero as the number of emitted neutrons increases. Angular momentum distributions were deduced (a) for each product prior to γ decay and (b) for the initial compound nuclei which lead to each product. In each case these were found to overlap extensively for several neighboring neutron numbers. The J distribution in ^{163}Yb extends up to $J \simeq 85$ prior to γ decay. At the higher energies α emission plays an important role in the deexcitation process by removing on the average an angular momentum of $\sim 10\hbar$. The present results suggest that α emission follows neutron evaporation. The J distributions obtained are compared with the predictions of the Bass model for fusing collisions. For the lower energies excellent agreement is observed. For the higher energies the Bass model prediction exceeds the measured xn and $xn\alpha$ cross sections at all J, indicating that other exit channels account for an appreciable fraction of the fusion cross section.

[NUCLEAR REACTIONS ^{150}Nd(^{20}Ne, $xn\gamma$), ^{150}Nd(^{20}Ne, $xn\alpha\gamma$), $x = 5-10$, $E = 127.7-172.4$ MeV; measured $\sigma(E, E_\gamma)$, γ-ray multiplicities; deduced J distributions in evaporation residues. Enriched target.]

I. INTRODUCTION

In recent years the limiting angular momentum $\hbar l_{crit}$ for fusion of target nuclei with heavy-ion projectiles has been extensively investigated via experiments designed to measure the cross section σ_{CF} for complete fusion.[1] The sharp cutoff approximation is usually used to obtain an adequate estimate of l_{crit} via $\sigma_{CF} = \pi \lambda\!\!\!^{-2} l_{crit}(l_{crit}+1)$. Values of l_{crit} upward of 60 have been reported for reactions involving medium and heavy product nuclei.[2,3] If complete fusion is assumed to be the same as compound-nucleus formation, then the deexcitation process will involve either fission or evaporation of light particles, the latter leading to the so-called evaporation residues.[4] The cross section σ_{ER} for such events leads, via a similar sharp cutoff approximation, to values of l_{ER} prior to particle emission; these have also been found to be greater than 60 for many systems.[2-4] Recently, Zebelman *et al.*[3] have measured the fusion cross sections for the formation of the ^{170}Yb compound nucleus at 107 MeV of excitation energy in reactions involving a variety of projectiles. For ^{11}B, ^{12}C, ^{16}O, and ^{20}Ne they reported values of (40 ± 3), (46 ± 4), (58 ± 4), and (63 ± 6) for l_{crit}, respectively. Since the fission cross sections[3] were observed to be small the l_{ER} values for the above reactions do not differ significantly from l_{crit}.

Although these large values of angular momentum are imparted to the evaporation residues, bound states with J values in excess of 22 have not as yet been observed by means of spectro-

scopic studies. The dissipation of the large amounts of angular momentum from the evaporation residues can be studied by measurement of the number of γ rays (multiplicity) in the cascades by which the reaction products deexcite. Multiplicity measurements for γ cascades that include the continuum region have been reported by Tjøm *et al.*[5] and by der Mateosian, Kistner, and Sunyar.[6] More recently, Hagemann *et al.*[7] have employed a multiple counter arrangement to study not only the average multiplicity, but also the higher moments of the multiplicity distribution.

The present investigation was undertaken to obtain information on the role of angular momentum in heavy-ion induced reactions. In particular we focus our attention on the following questions: (a) How is the angular momentum of the initial compound nucleus distributed on the average among the reaction products? (b) Can the spin distributions of the various evaporation residues prior to γ-ray emission be deduced? If so, is there evidence for a lower cutoff in the J distribution? (c) How does the average angular momentum imparted to each of the evaporation residues vary with the initial excitation energy?

In the present experiments the reactions of ^{20}Ne incident on ^{150}Nd were studied at four energies from 127.7 to 172.4 MeV, corresponding to excitation energies in the initial ^{170}Yb compound nucleus of 92.7, 107.1, 123.3, and 132.2 MeV. All possible coincidences between one Ge(Li) spectrometer and eight NaI(Tl) detectors were recorded. From these measurements the average multiplicity, the standard deviation, and the skewness of the multiplicity distribution for most of the reaction products were deduced. In addition, the cross sections for producing the various products were measured. Comparison of these results with those from fusion cross section measurements permits one to deduce the spin distributions in all identified products.

II. MULTIPLICITY DISTRIBUTION

The deexcitation pattern of a γ cascade following a nuclear reaction induced by heavy projectiles proceeds via a large number of highly excited states. Cascades with widely varying numbers of γ rays are possible so that wide distributions in multiplicity may be expected.

The method employed in extracting the moments of multiplicity distribution is similar to that of Hagemann *et al.*[7] but several extensions and generalizations have been included so that the present method will be outlined in some detail.

A. Multiplicities of the incoming transitions

For simplicity we shall discuss first the case of a cascade of M_{in} γ rays entering the highest (ith) state of the ground state band with angular momentum J. The ith state (spin J) then deexcites via a sequence of transitions with $J \to J-2 \to J-4 \to \cdots \to J_g$, where J_g is the angular momentum where the observed cascade terminates. More complex situations for levels with side feeding and/or with branched decays can be analyzed by making use of the known decay scheme and the intensity pattern for the side feeding as discussed in Sec. II B below. Consider now the γ ray ($J \to J-2$) from the ith level. This is detected in the Ge(Li) detector with a singles rate [ignoring for the time being summing effects in the Ge(Li) detector] given by

$$Q_s^{(i)} = \sigma_i \Omega_{\mathrm{Ge}}^{(i)} , \tag{1}$$

where σ_i is the cross section leading to the ith state and $\Omega_{\mathrm{Ge}}^{(i)}$ is the efficiency of the Ge(Li) detector, including solid angle, for the full energy peak. The detection of this γ ray provides the "gate event" and coincidences out of the N identical NaI(Tl) detectors are examined. The counting rate for a p-fold coincidence from all possible combinations of p detectors that fire is

$$Q_{c,p}^{(i)} = \sigma_i \Omega_{\mathrm{Ge}}^{(i)} P_{Np}^{(i)} , \tag{2}$$

where $P_{Np}^{(i)}$ is the overall probability that out of N detectors p of them fire. The quantity $P_{Np}^{(i)}$, of course, must account for the probability that any NaI detector recorded one or more photons and for the fact that for each cascade there is a definite angular correlation function. This gives a certain probability for a p-fold coincidence to represent more than p photons. Ignoring, for the moment, the angular correlation effects we note that the probabilities $P_{Np}^{(i)}$ can be obtained from experiment as $Q_{c,p}^{(i)}/Q_s^{(i)}$, or as the ratios

$$P_{Np}^{(i)} = \sum_{\beta} C_{p\beta}^{(i)} \Big/ \sum_{p=0}^{N} \sum_{\beta} C_{p\beta}^{(i)} , \tag{3}$$

where $C_{p\beta}^{(i)}$ are the peak areas corresponding to a particular set of detectors β that registered p-fold coincidences.

Assuming isotropic γ-ray and neutron emission one can show[8] that

$$P_{Np}^{(i)} = \binom{N}{p} \sum_{k=0}^{p} (-1)^{k-p} \binom{p}{k} F_k^{(i)} , \tag{4}$$

where

$$F_k^{(i)} = [1 - (N-k)\bar{\Omega}]^{M_{in}} K_{N-k}^{(i-1)} K_{N-k}^{(\mathrm{neut})} , \tag{4a}$$

with

$$K_{N-k}^{(i-1)} = \prod_j [1 - (N-k)\Omega_j] \tag{4b}$$

to be evaluated from the $(i-1)$th state down to the ground state (numbered as 0), using the known NaI γ-ray efficiencies Ω_j, and

$$K_{N-k}^{(\text{neut})} = [1 - (N-k)\Omega_{\text{neut}}^{(x)}]^x \tag{4c}$$

representing the neutron response of one of the NaI detectors having an average efficiency $\Omega_{\text{neut}}^{(x)}$ for neutron detection when the number of emitted neutrons is x. The average efficiency $\bar{\Omega}$ refers to the cascade of M_{in} γ rays entering the state i. The probabilities evaluated via Eqs. (4) correctly account for losses due to coincidence summing in the NaI counters.

In order to extract the moments of the multiplicity distribution one can follow two methods. In the first one, the P method, the first term in $F_k^{(i)}$ of Eq. (4a) is expanded in powers of $\bar{\Omega}$ to give via Eq. (4)

$$\sum_{r=1}^{M_{in}} \rho_{pr}^{(i)} X_r^{(i)} = P_{Np}^{(i)} - (1 + \rho_{p0}) , \tag{5}$$

where

$$\rho_{pr}^{(i)} = \binom{N}{p} \frac{1}{r!} \sum_{k=0}^{p} (-1)^{k-p+r} \binom{p}{k} (N-k)^r K_{N-k}^{(i-1)} K_{N-k}^{(\text{neut})} \tag{5a}$$

and

$$X_r^{(i)} = \langle M_{in}(M_{in}-1)\cdots(M_{in}-r+1)\rangle (\bar{\Omega})^r . \tag{5b}$$

For a sufficiently high value $p_{\max}$ of the highest-fold observed, Eqs. (5) can be solved to give a good approximation of $X_r^{(i)}$, with $r = 1, 2, \ldots, p_{\max}$ by setting $M_{in} = p_{\max}$.

In the second method, the R method, one can add the experimental $P_{Np}^{(i)}$ values to obtain the experimental $R_p^{(i)} \equiv P_{pp}^{(i)}$ values via

$$R_p^{(i)} = \left[\binom{N}{p}\right]^{-1} \sum_{k=p}^{N} \binom{k}{p} P_{Nk}^{(i)} . \tag{6}$$

The quantity $R_p^{(i)}$ represents the probability for observing a p-fold coincidence event if only p-NaI(Tl) detectors were present. It is easy to show that

$$R_p^{(i)} = \sum_{k=0}^{p} (-1)^k \binom{p}{k} (1 - k\bar{\Omega})^{M_{in}} K_k^{(i-1)} K_k^{(\text{neut})} , \tag{7}$$

where

$$K_k^{(i-1)} = \prod_j (1 - k\Omega_j) \text{ and } K_k^{(\text{neut})} = (1 - k\Omega_{\text{neut}}^{(x)})^x . \tag{7a}$$

Expanding Eq. (7) in powers of $\bar{\Omega}$ one obtains now

$$\sum_{r=1}^{M_{in}} \lambda_{pr}^{(i)} X_r^{(i)} = R_p^{(i)} - (1 + \lambda_{p0}) , \tag{8}$$

where

$$\lambda_{pr}^{(i)} = \frac{1}{r!} \sum_{k=1}^{p} (-1)^{k+r} \binom{p}{k} k^r K_k^{(i-1)} K_k^{(\text{neut})} \tag{8a}$$

with $X_r^{(i)}$ given by Eq. (5b).

Again, setting $M_{in} = p_{\max}$ permits one to solve Eqs. (8) for $X_r^{(i)}$, with $r = 1, 2, \ldots, p_{\max}$.

One advantage of the R method is that it allows one to observe the magnitude of the corrections for coincidence summing effects in each NaI detector from all higher-folds $(p+1, p+2, \ldots, p_{\max})$ to each X_p value.[7]

From the $X_r^{(i)}$ values the moments of the multiplicity distribution can be obtained provided the detection efficiencies $\bar{\Omega}$ are known. In general

$$\bar{\Omega} = \Omega_\gamma (1+\alpha)^{-1} (1 - \Omega_0)^{-1} , \tag{9}$$

where Ω_γ is the overall efficiency (full energy and Compton distribution) of one of the N identical NaI(Tl) counters, α is the total conversion coefficient, and Ω_0 is the overall efficiency of the Ge(Li). The last factor in Eq. (9) as far as the multiplicity is concerned corrects[7] for coincidence summing effects in the Ge(Li) detector. In the present experiments $\Omega_0 \simeq 0.006$.

If angular correlation corrections are to be included, a reasonable approximation can be obtained by ignoring coincidence summing effects in the NaI detector which in this work were found to vary between 5 and 12%. In this case it is sufficient to divide the experimental peak areas $[\sum_\beta C_{p\beta}^{(i)}]$ of Eq. (3) for $p \geq 1$ by $\bar{W}_p^{(i)}$ given by

$$\bar{W}_p^{(i)} = \left[\binom{N}{p}\right]^{-1} \sum_\beta W_{p\beta}^{(i)}(\theta_{\text{Ge}}, \ldots, \theta_p) , \tag{10}$$

where $W_{p\beta}^{(i)}$ are the p-fold correlation functions corresponding to a given set β of the p detectors that fired.

From the $X_r^{(i)}$ values the mean values $\langle M_{in}\rangle, \langle M_{in}{}^2\rangle, \ldots, \langle M_{in}{}^{p_{\max}}\rangle$ can be determined from Eqs. (5b) and these in turn can be used to calculate the higher moments

$$\mu_n = \langle (M_{in} - \langle M_{in}\rangle)^n \rangle$$

of the distribution of M_{in} around the average $\langle M_{in}\rangle$.

B. Multiplicities of side feeding

When unresolved cascades populate observed levels (side feeding) in the reaction products then the moments of the multiplicity distribution for the side feeding into the ith level can be determined from measurement of the $P_{Np}^{(i)}$ probabilities for a given gating γ ray deexciting the ith level and populating the jth level below. In what follows the jth level may decay by branching to several levels below and the ith level may be

populated by several incoming transitions.

In this case Eqs. (8) can be modified to read

$$\sum_{r=1}^{p_{\max}} \lambda_{pr}^{(i)} X_r^{(i)} = \frac{1}{f_{\mathrm{SF}}^{(i)}} [R_p^{(i\to j)} - A_p^{(i\to j)}] - (1+\lambda_{p0}) , \tag{11}$$

where $A_p^{(i\to j)}$ accounts for the coincidence probability via known (earlier measured) cascades connecting from above and below to the gating transition, and $f_{\mathrm{SF}}^{(i)}$ is the side-feeding fraction entering the ith state.

The detailed evaluation of $A_p^{(i\to j)}$ now depends on the particular decay scheme in each case. For a level i it is given by

$$A_p^{(i\to j)} = \sum_{k=0}^{p} (-1)^k \binom{p}{k} L_k^{(i)} K_k^{(j)} K_k^{(\mathrm{neut})} , \tag{12}$$

where

$$L_k^{(i)} = \sum_{m=i+1}^{l} f_{mi}(1 - k\Omega_{mi}) [L_k^{(m)} + f_{\mathrm{SF}}^{(m)} (1 - k\overline{\Omega}_{\mathrm{SF}}^{(m)})^{M_{\mathrm{SF}}^{(m)}}] , \tag{12a}$$

$$K_k^{(j)} = \sum_{q=0}^{j-1} b_{jq} (1 - k\Omega_{jq}) K_k^{(q)} , \tag{12b}$$

and

$$K_k^{(\mathrm{neut})} = [1 - k\Omega_{\mathrm{neut}}^{(x)}]^x . \tag{12c}$$

In Eq. (12a) l is the highest discrete state resolved. The feeding fractions f_{mi} from the states m above into the state i and the side feeding fraction satisfy

$$f_{\mathrm{SF}}^{(i)} + \sum_{m=i+1}^{l} f_{mi} = 1 .$$

The NaI(Tl) efficiencies between observed bound states in (12a) and (12b) are labeled by the subscript denoting the initial and final state. The decay branching ratios b_{jq} for the deexcitation of the state j to states q below also are normalized such that

$$\sum_{q=0}^{j-1} b_{jq} = 1 .$$

In the recurrence relation (12b) the ground state is numbered as 0 and $K_k^{(0)} = 1$, $K_k^{(1)} = (1 - k\Omega_{10})$, etc. In Eq. (12a) $M_{\mathrm{SF}}^{(m)}$ and $\overline{\Omega}_{\mathrm{SF}}^{(m)}$ are the average multiplicity and average γ-ray efficiency for the side feeding entering the state m. In order to determine the moments of the distribution of $M_{\mathrm{SF}}^{(i)}$ the observed levels must be analyzed downward starting from the top level l. It is clear that as one proceeds downward the uncertainties increase progressively since $f_{\mathrm{SF}}^{(i)}$ decreases and the errors from the highest levels propagate downward.

III. EXPERIMENTAL METHODS

Eight 5.1 cm diameter by 7.6 cm long NaI(Tl) detectors were placed at a distance of 10 cm from the target, each with its symmetry axis passing through the target center. A lead shield was cast that could support up to seven NaI(Tl) detectors with one positioned at 90° to the beam in the horizontal plane and six additional ones equally spaced on a cone of half angle of 45° coaxial with the 90° detector. This arrangement allows for detectors at 45°, 90°, and 135° to the beam in the horizontal reaction plane with two others above and two below this plane. Only three of the possible four out-of-plane positions were used in this experiment. Two additional NaI(Tl) detectors were located in the horizontal plane at −50° and −140° to the beam direction. A 15% Ge(Li) detector was placed at −90° to the beam in the horizontal plane at a distance of 8.5 cm from the target. The resolution (full width at half maximum) was 3.5 keV at 1332 keV. The minimum lead shielding between adjacent NaI(Tl) detectors or the Ge(Li) and the neighboring NaI(Tl) detectors was 2 cm, which is sufficient to eliminate most of the crystal-to-crystal scattering.

The target was a uniform 1.3 mg/cm^2 self-supporting ^{150}Nd foil, enriched to 96% in mass 150, mounted on a thin Al holder at 30° off the vertical direction to permit visibility to all detectors. Beams of ^{20}Ne^{6+} were provided by the Oak Ridge isochronous cyclotron. The center-target energies were 127.7, 144.0, 163.5, and 172.4 MeV.

To avoid detection of Nd x rays and to make $\overline{\Omega}$ less dependent on γ-ray energy, 0.5 mm Cd and 0.13 mm Cu absorbers were placed in front of each NaI(Tl) detector. In addition, the lower level discriminator thresholds were set to accept pulses $\geq$ 75 keV.

The overlap coincidence technique was employed. The Ge(Li) timing signal was derived from a constant-fraction discriminator operated in the slow-rise-time-rejection mode. The Ge(Li) and NaI(Tl) timing signals were each adjusted to a width of 35 ns, resulting in a resolving time of 70 ns. This was sufficient to cover the amplitude dependence of the timing from the Ge(Li) detector, thus ensuring the same triggering efficiency in the 0-fold and the higher-fold coincidences. The rf microstructure of the beam consisted of beam bursts 3 to 4 ns wide 129 to 135 ns apart. Thus the resolving time was adequate to reject accidental coincidences from adjacent beam bursts. For total Ge(Li) rates of 2000 cps an overall 1-fold random fraction of $\leq$ 0.3% was achieved for γ-ray multiplicities of 20.

In these experiments 8192-channel Ge(Li) spectra corresponding to 0-fold up to 8-fold coincidences were stored on disk by use of an on-line computer. The spectra obtained for 2-fold and higher coin-

cidences consisted of all possible combinations of each fold. The eight 1-fold spectra were recorded separately and were summed later.

The NaI(Tl) counters with the Cd and Cu absorbers were calibrated for total efficiency with standard γ-ray sources of ^{109}Cd, ^{57}Co, ^{137}Cs, ^{54}Mn, and ^{60}Co. A ^{133}Ba source was also used to provide a point at $\simeq$340 keV. The overall efficiency of the NaI(Tl) was found to be rather insensitive to γ-ray energy, varying from its maximum value of 0.0114 at 250 keV to 0.010 at 600 keV and 0.0087 at 1250 keV. Sources with simple cascades such as ^{60}Co and ^{88}Y were used in multiplicity measurements before and after the run to check the apparatus.

The Ge(Li) detector efficiency was calibrated absolutely for the full energy peak. Although this information is not needed for the multiplicity measurements, it permitted the determination of the cross sections for the formation of the various identified reaction products from measurement of the integrated beam current and the target thickness.

The crystal-to-crystal [Ge(Li)-NaI and NaI-NaI] scattering in the present apparatus was checked with sources of ^{137}Cs or ^{54}Mn in coincidence (1-fold) and ^{60}Co or ^{88}Y in 2-fold coincidence. In all cases this effect was found negligible.

In order to correct for the response of the NaI(Tl) detectors to neutrons, the efficiency of the NaI(Tl) for neutron detection relative to that for γ rays was determined in separate experiments at the Washington University cyclotron using the ^{95}Mo$(\alpha,n\gamma)$ ^{98}Ru reaction at 14.0 MeV. First, the average multiplicity of all γ-ray cascades was obtained using the same apparatus. The response to neutrons was then determined in a time-of-flight experiment. One of the NaI(Tl) detectors was placed at 5 cm from the target and a second one at 98 cm from the target. The latter provided the start pulses and the stop pulses were derived from the cyclotron rf. The detector at 5 cm served to impose a coincidence requirement in order to reduce the background of the time-of-flight spectrum. The result obtained was $(14\pm4)\%$ of the γ-ray efficiency for an average γ-ray energy of $\simeq$700 keV and a measured most probable neutron energy of $\simeq$2.6 MeV. The average energies for neutrons and γ rays under the conditions of this determination do not differ substantially from those in the ^{20}Ne + ^{150}Nd experiments[9] so that the constant efficiency of $\Omega^{(x)}_{neut} = 0.0014 \pm 0.0005$ was used in the analysis of the present results.

IV. RESULTS

A set of spectra recorded with the Ge(Li) detector in 0-, 1-, 2-, 3-, 4-, and (5–8)-fold coincidence is shown in Fig. 1. The (5–8)-fold is the sum of 5-, 6-, 7-, and 8-fold spectra. These are from the 127.7 MeV ^{20}Ne bombardment of ^{150}Nd. It is interesting to note that the 0-fold spectra contain considerable amounts of background and low multiplicity radiations. In Fig. 1 one also notices the increasing intensity of the $(^{20}\mathrm{Ne},6n)$ radiations relative to those from the $(^{20}\mathrm{Ne},7n)$ and $(^{20}\mathrm{Ne},8n)$ as one progresses to higher-fold coincidences. From the peak areas in each p-fold spectrum, which arise from the sum of all possible combinations of p NaI detectors, the probabilities $P^{(i)}_{Np}$ were extracted for every bombardment energy. These are summarized in Table I (E_{lab} = 127.7 and 144.0 MeV) and Table II (E_{lab} = 163.5 and 172.4 MeV). The first three columns in Tables I and II give the product nucleus and particles emitted, the observed transition energy in keV, and the angular momentum J of the state deexcited by the gating transitions. Columns 4–8 and 10–14 in Tables I and II give the $P^{(i)}_{Np}$ values for $p = 0$, 1, 2, 3, and 4 without the correction for angular correlation effects. Columns 9 and 15 in Tables I and II give the probabilities corresponding to the sum of 5- through 8-fold coincidences.

A. Available γ-ray energy

In order to extract multiplicities from the results of Tables I and II the efficiency $\bar{\Omega}$ of Eq. (9) must be known, and the quantity $\bar{W}_p(i)$ evaluated. The first of these depends on the average γ-ray energy in the cascade. In the present experiments products were identified corresponding to the emission of 5–8 or 7–10 neutrons depending on the bombardment energy. For a given gating transition in a given product nucleus the total available energy defined as $(E_{c.m.}+Q)$ can be easily calculated. For the $^{170-x}$Yb products this energy must be partitioned into the total kinetic energy $\langle E_n \rangle$ of x emitted neutrons and the average total γ-ray energy $\langle T'_\gamma \rangle = \langle T_\gamma \rangle + E^{(i)}_{level}$, where $E^{(i)}_{level}$ is the excitation energy of the ith level. Once the total γ-ray energy $\langle T_\gamma \rangle = \langle M_{in} \rangle \langle E_\gamma \rangle$ is known a solution for $\langle M_{in} \rangle$ via Eqs. (8) or (11) can be obtained by iteration. One first assumes an $\langle M_{in} \rangle$, obtains $\langle E_\gamma \rangle$ and thus $\bar{\Omega}$, and then calculates $\langle M_{in} \rangle$ via Eqs. (8) or (11). Since $\bar{\Omega}$ is a piecewise monotonic function of E_γ over the entire region of interest, a unique solution is always obtained. A reasonable method for dividing the available energy into $\langle T'_\gamma \rangle$ and $\langle E_n \rangle$ is to use the results of Alexander and Natowitz,[10] who give $\langle T'_\gamma \rangle = a + b(E_{c.m.}+Q)$. They obtain the coefficients a and b by analysis of differential recoil range data from a wealth of nuclear reactions induced by heavy ions ranging from $(^{12}\mathrm{C},3n)$ up to $(^{20}\mathrm{Ne},9n)$ and leading to Dy final

nuclei. The observed independence of this partition on entrance and exit channel[10] suggests the use of these equations for the (^{20}Ne,xn) reactions leading to Yb nuclei. For the (^{20}Ne,$xn\alpha$) reactions the ($E_{c.m.}+Q$) values for the $^{166-x}$Er nuclei were calculated assuming an average α-particle energy

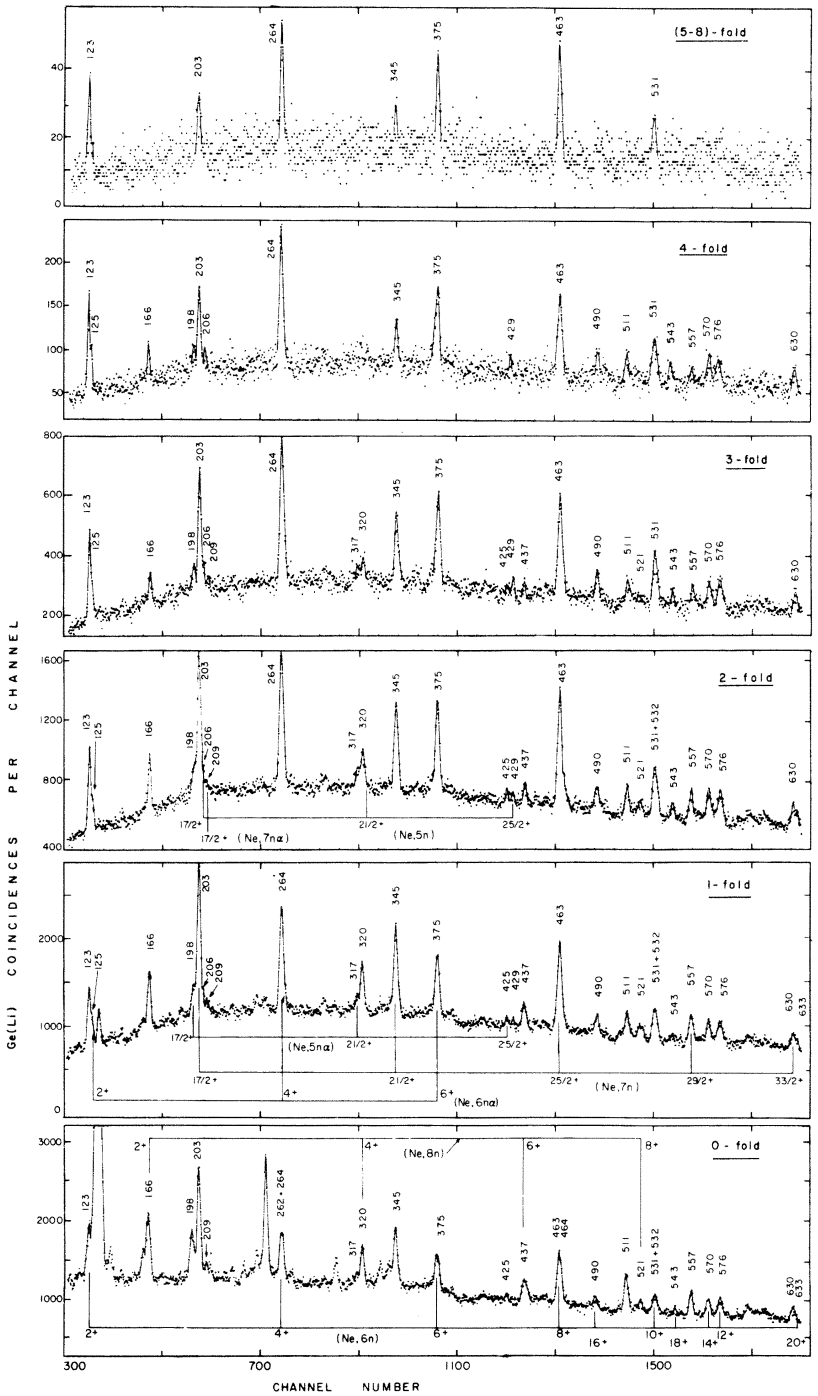

FIG. 1. Spectra recorded with a Ge(Li) γ-ray detector in multiple coincidence with eight NaI(Tl) detectors from a 127.7 MeV ^{20}Ne bombardment of ^{150}Nd. The 0-fold refers to no coincidence and the (5–8)-fold refers to the sum of 5- through 8-fold coincidences. The higher-fold spectra show enhanced intensities for the γ rays associated with the higher multiplicity cascades which occur in the reactions emitting fewer neutrons.

TABLE I. Multiple coincidence probabilities $P_{8p}^{(i)}$ from the reactions of 127.7 and 144.0 MeV ^{20}Ne with ^{150}Nd. The underlined numbers are estimates of the statistical error and refer to the least significant figures indicated.

Final product	E_γ (keV)	State J	P_{8p} (×100) E_{lab} = 127.7 MeV 0-fold	1-fold	2-fold	3-fold	4-fold	(5–8)-fold	P_{8p} (×100) E_{lab} = 144.0 MeV 0-fold	1-fold	2-fold	3-fold	4-fold	(5–8)-fold
^{165}Yb + 5n	206	$\frac{17}{2}^+$	19 9	37 7	28 6	14 3	2.7 11	0.2 6						
	429	$\frac{25}{2}^+$	12 3	28 6	34 7	20 4	4.0 10	1.3 4						
^{164}Yb + 6n	123	2^+	26 5	34 2	24.7 16	11.1 7	3.8 2	0.93 12	18.9 41	38 6	28 6	9.1 31	4.3 8	1.5 8
+ (^{160}Er + 6$n\alpha$)	262	4^+	17.3 9	36.4 9	27.9 8	13.5 5	4.1 2	0.79 9	15.2 16	35 2	30.0 8	14.1 10	5.1 6	0.66 4
	375	6^+	22.2 11	33.5 12	26.8 11	12.6 7	4.0 3	0.84 13	14.8 24	36.3 44	30.33 1	13.3 19	4.5 13	0.74 45
	463 [a]	8^+	23.0 9	35.5 10	26.9 9	10.7 4	3.1 2	0.79 11	20.1 18	34.8 20	25.9 16	12.7 14	5.6 6	0.87 19
	531	10^+	17.8 16	33.2 23	29.9 22	14.0 13	4.2 2	0.87 20	13.0 26	40.3 32	26.1 26	14.7 15	5.0 8	0.87 50
	577	12^+	24.0 20	30.5 24	27.1 20	13.6 13	3.8 6	1.03 16	17.4 23	35.6 26	29.3 25	12.4 20	4.5 8	0.92 43
	570	14^+	25.3 21	29.9 24	28.4 21	11.9 12	3.9 6	0.56 15	13.2 31	36.4 43	31.2 40	13.4 31	4.9 12	0.85 43
	490	16^+	20.6 46	34.0 40	27.5 40	12.8 19	3.4 10	1.7 5						
	543	18^+	20 7	23 7	28 7	18 4	10 2	1.1 6						
	633	20^+	26 5	28 12	27 6	10 4	6 3	3 2						
^{163}Yb + 7n	203	$\frac{17}{2}^+$	31.1 11	37.4 11	21.7 7	7.7 4	1.7 1	0.33 11	23.7 11	33.0 15	26.6 11	12.1 6	3.96 29	0.71 8
	345	$\frac{21}{2}^+$	29.5 21	37.3 16	23.4 9	8.1 5	1.6 2	0.21 7	21.8 15	31.8 19	26.2 15	15.3 11	4.3 5	0.63 31
	463 [a]	$\frac{25}{2}^+$	23.0 9	35.5 10	26.9 9	10.7 4	3.1 2	0.79 11	20.3 18	35.2 21	26.2 16	12.8 14	4.5 6	0.88 19
	557	$\frac{29}{2}^+$	31.7 23	37.0 25	21.3 19	7.4 11	2.4 5	0.22 13						
	630	$\frac{33}{2}^+$	39 7	26 8	22 4	7.1 34	5.0 11	0.94 64						
	680	$\frac{37}{2}^+$	21 7	46 26	24 12	9.7 32								
^{162}Yb + 8n	166	2^+	45.8 18	34.3 14	14.6 8	4.2 4	1.07 27	0.08 4	28.0 11	34.1 9	23.9 7	10.4 4	2.9 2	0.68 23
	320	4^+	35.9 29	40.5 39	20.3 19	2.5 8	0.79 37		20.9 9	36.8 11	26.9 8	11.8 5	3.0 2	0.66 9
	437	6^+	45.7 59	35.8 52	13.5 29	3.9 13	1.0 4		20.7 13	37.7 13	26.7 11	11.1 7	3.1 4	0.77 11
	521	8^+	41.4 41	35.2 44	16.9 35	5.8 20	0.55 37	0.09 9						
^{161}Yb + 9n	232	$\frac{17}{2}^+$							41.5 78	37.8 53	16.7 37	3.2 7	0.69 28	0.14 7
^{161}Er + 5$n\alpha$	317	$\frac{21}{2}^+$							26 6	38 6	34 6	1.6 3		
	425	$\frac{25}{2}^+$							23 5	31 7	34 8	9.4 27	1.8 6	0.5 2
^{159}Er + 7$n\alpha$	209	$\frac{17}{2}^+$							39 3	32 3	20 2	6.7 10	1.6 5	0.28 19
	350	$\frac{21}{2}^+$							35 5	35 5	18 3	10.1 25	2.2 11	0.35 35
^{158}Er + 8$n\alpha$	193	2^+							45 7	31 5	21 4	3.0 10		
	444	6^+							40 9	29 7	23 5	7.8 27		

[a] Unresolved doublet.

TABLE II. Multiple coincidence probabilities $P_{8p}^{(i)}$ from the reactions of 163.5 and 172.4 MeV ^{20}Ne with ^{150}Nd.

Final product	E_γ (keV)	State J	P_{8p} (×100) E_{lab} = 163.5 MeV 0-fold	1-fold	2-fold	3-fold	4-fold	(5–8)-fold	P_{8p} (×100) E_{lab} = 172.4 MeV 0-fold	1-fold	2-fold	3-fold	4-fold	(5–8)-fold
^{163}Yb +7n	203	$\frac{17}{2}^+$	15 7	30 8	32 7	19 5	4.2 10	1.2 6	13 5	31 10	25 9	19 7	7.3 20	4.7 19
	345	$\frac{21}{2}^+$	19 12	25 7	26 7	12.6 50	12.5 76	4.7 20						
^{162}Yb +8n	166	2^+	21.3 23	35.0 20	24.8 12	13.2 7	4.5 3	1.25 15	14.6 46	29.8 45	31.4 65	17.5 47	4.8 14	2.0 7
	320	4^+	8.6 22	31.9 20	32.2 19	18.8 11	6.4 6	2.1 3	8.2 23	25.2 41	34.5 40	21.4 23	9.2 15	1.5 4
	437	6^+	18.1 25	36.5 21	26.9 13	13.5 12	4.2 7	0.7 4	12.3 52	30.4 55	27.4 57	25.1 35	3.4 13	1.4 6
^{161}Yb +9n	232	$\frac{17}{2}^+$	22.7 24	36.4 22	26.0 15	10.1 8	3.0 5	0.18 2	20.4 45	33.7 29	27.2 24	13.1 15	4.5 7	1.0 2
^{160}Yb +10n	243	2^+	36.3 41	44.9 55	13.8 16	4.4 4	0.54 38		28.0 46	35.6 27	23.2 19	10.2 11	2.7 5	0.33 7
	395	4^+	26.4 16	35.4 16	25.4 15	9.8 7	2.4 3	0.52 15	28.6 20	39.2 25	14.0 19	14.0 13	3.7 5	0.68 13
	589	8^+	18.0 42	37.3 52	32.8 43	11.9 23			23.8 35	33.0 61	25.5 44	13.2 24	3.7 18	0.85 31
^{159}Er +7$n\alpha$	209	$\frac{17}{2}^+$	23.2 21	32.7 30	27.4 26	12.5 17	3.4 7	0.81 51	21.2 56	30.7 60	30.4 45	12.0 33	4.5 6	1.2 3
	350	$\frac{21}{2}^+$	22.9 37	29.1 39	23.6 63	15.7 42	6.2 31	2.5 8	23.0 55	24.6 48	29.5 58	13.7 24	6.7 19	2.6 16
^{158}Er +8$n\alpha$	193	2^+	22.4 15	36.9 16	25.8 14	11.0 7	2.9 3		21.0 18	34.8 23	26.4 14	11.6 8	5.1 4	1.2 2
	336	4^+	29.0 13	23.0 19	25.0 13	14.9 10	6.7 8	1.4 4	28.0 25	33.2 23	23.1 19	11.6 10	3.6 6	0.54 17
	444	6^+	21.4 30	41.5 28	25.0 17	9.4 13	2.7 8		23.5 36	35.0 35	22.7 25	13.9 16	3.5 9	1.3 4
^{157}Er +9$n\alpha$	266	$\frac{17}{2}^+$	37.0 43	46.3 68	8.9 19	6.6 16	1.25 82		35.9 85	33.3 36	20.7 25	8.1 16	1.9 7	0.12 12
	415	$\frac{21}{2}^+$	34.0 50	34.3 47	21 5	8.6 21	2.0 9	0.1 1	34.1 35	36.2 35	20.1 27	7.3 16	2.4 8	
^{156}Er +10$n\alpha$	453	4^+							40 7	36 6	12.5 33	9.3 23	1.6 10	0.6 4

TABLE III. Summary of the level cross sections, average multiplicity $\langle M_J \rangle$, width σ_{M_J} and skewness $s_{M_J} = \mu_3/\sigma_{M_J}^3$ of the multiplicity distribution for the γ cascades in the reaction products from bombardments of ^{150}Nd with 127.7 and 144.0 MeV ^{20}Ne.

			E_{lab} = 127.7 MeV					E_{lab} = 144.0 MeV				
Final product	E_γ (keV)	J^π Level	σ_J [a] (mb)	$\langle E_\gamma \rangle$ (MeV)	$\langle M_J \rangle$	σ_{M_J}	s_{M_J}	σ_J [b] (mb)	$\langle E_\gamma \rangle$ (MeV)	$\langle M_J \rangle$	σ_{M_J}	s_{M_J}
^{165}Yb + 5n		$\frac{13}{2}^+$	(45 6)									
	206	$\frac{17}{2}^+$	36 4	1.49	24.3 38							
	429	$\frac{25}{2}^+$	20 2	1.12	28.6 28							
^{164}Yb + 6n		0^+	(431 44) [c]					(154 21)				
+ (^{160}Er + 6$n\alpha$)	123	2^+	382 22	1.14	21.6 6	8.5 18	−1.1 28	107 21	1.46	24.0 25	7.4 92	2.9 236
	262	4^+	329 11	1.03	24.4 4	3.2 30	−6.2 383	138 5	1.35	26.6 7		
	375	6^+	276 11	1.12	23.4 5	6.8 19	−2.7 48	144 8	1.41	26.2 17		
	463 [d]	8^+	219 33	1.23	22.1 4	6.1 14	−0.7 38		1.52	25.4 9	7.7 36	−2.6 71
	531	10^+	193 8	1.10	24.8 9	3.5 60		112 5	1.48	26.5 13		
	577	12^+	158 7	1.22	23.4 9	8.0 27	−2.7 47		1.61	25.4 14	4.3 86	−1.54 77
	570	14^+	150 6	1.33	22.5 10	7.1 30	−4.6 76	104 7	1.56	26.6 21		
	490	16^+	91 7	1.27	23.8 17	8.1 48	0.25 622					
	543	18^+	43 6	1.00	28.5 32	8.8 94	−7.4 270					
	633	20^+	63 9	1.34	24.2 36	13.5 66	−0.29 309					
^{163}Yb + 7n		$\frac{13}{2}^+$	(483 54)					(298 41)				
	203	$\frac{17}{2}^+$	369 6	0.87	16.4 3	5.8 11	−0.6 29	228 6	1.11	22.2 5	7.1 17	−2.9 44
	345	$\frac{21}{2}^+$	284 8	0.87	16.9 4	4.3 18	−3.9 93	163 6	1.08	23.6 8	6.3 34	−7.0 149
	463 [d]	$\frac{25}{2}^+$	215 32	0.74	19.9 3	5.7 13	−0.6 36		1.12	23.2 9	6.7 35	−2.3 88
	557	$\frac{29}{2}^+$	161 7	0.95	16.6 8	6.4 25	−0.9 42					
	630	$\frac{33}{2}^+$	112 13	0.91	17.5 22	12.3 35	−0.35 165					
	680	$\frac{37}{2}^+$	90 26	0.92	17.6 50							
^{162}Yb + 8n		0^+	236 27 [b]					(478 30)				
	166	2^+	202 5	0.55	10.8 4	6.0 9	0.14 142	454 7	0.86	19.0 3	7.5 12	−1.1 22
	320	4^+	127 10	0.49	12.4 8			413 8	0.80	20.7 3	3.9 20	−1.4 133
	473	6^+	99 8	0.58	10.9 11	5.3 26	0.2 38	346 7	0.83	20.7 5	4.4 26	2.1 128
	521	8^+	79 5	0.50	12.1 13	4.9 36	−2.1 79					
^{161}Yb + 9n	232	$\frac{17}{2}^+$						66 5	0.59	11.2 12	3.7 45	3.6 200
^{161}Er + 5$n\alpha$		$\frac{13}{2}^+$	(69 16)									
	317	$\frac{21}{2}^+$	41 4	1.18	16.9 19							
	425	$\frac{25}{2}^+$	31 3	0.97	20.9 28							
^{160}Er + 6$n\alpha$		0^+	(133 43) [e]					(52 20) [e]				
^{159}Er + 7$n\alpha$		$\frac{13}{2}^+$						(114 20)				
	209	$\frac{17}{2}^+$						92 5	0.93	15.1 9	7.6 22	−0.9 30
	350	$\frac{21}{2}^+$						49 4	0.87	16.6 17	8.2 42	−1.2 51
^{158}Er + 8$n\alpha$		0^+						(40 3)				
	193	2^+						38 3	0.56	10.9 13	2.2 69	
	444	6^+						44 5	0.49	13.2 18	3.9 63	

[a] Values obtained for the level yields from measurement of the γ rays at 90° corrected for $E2$ angular correlation by multiplying the 90° yield by 1.1. In the odd mass nuclei only the positive parity bands were resolved. The values given in parentheses for the $\frac{13}{2}^+$ of the 0^+ states were obtained by extrapolation and should represent a reasonable upper limit of the cross section for each evaporation residue.

[b] Cross section sum normalized to 1140 mb (see text).

[c] Cross sections given refer to the (^{20}Ne, 6n) + (^{20}Ne, 6$n\alpha$) products (see text).

[d] Close doublet, resolved by assuming equal contribution from the 6n and 7n products.

[e] Value estimated from the lower-fold coincidence spectra.

of 18 MeV, which is near the Coulomb barrier for α emission in this mass region. An increase of 2 MeV in $\bar{E}_\alpha$ will cause a decrease of 4% in $\langle M \rangle$ for the most sensitive reaction (^{20}Ne, $10n\alpha$).

B. Angular correlation effects

The angular correlation corrections $\bar{W}_p$ of Eq. (10) for the present data were estimated by considering the simplest case of $\bar{W}_1$ for a highly aligned high-spin cascade of stretched $E2$ transitions. One of its members was assumed to be observed in the Ge(Li) detector and another in one of the NaI detectors. For the present geometry a value of $\bar{W}_1 = 0.975 \pm 0.005$ was obtained, neglecting the summing effects. This result is rather insensitive to the degree of assumed nuclear spin alignment. The corrections for $p \geq 2$ are expected to be somewhat larger due to possible increase in alignment when several members of the casade are detected. In order to examine the effects of these corrections on the first three moments we have analyzed the present results assuming (a) $\bar{W}_1 = \bar{W}_2 = \cdots = \bar{W}_{p_{\max}}$ and (b) $\bar{W}_p = \bar{W}_1[1-(p-1)0.0125]$. We found that in case (b) $\langle M_{in} \rangle$, $\sigma_{M_{in}}$, and $s_{M_{in}}$ changed on the average by +1.3, +1.6, and −2.0% relative to the values obtained in case (a). The results of this work were corrected for angular correlation effects according to the approximation (b) above.

C. Cross sections

Before presenting the multiplicity results attention must be given to the observed decay pattern at each bombardment energy. In this work

TABLE IV. Summary of the level cross sections, average multiplicity $\langle M_J \rangle$, width σ_{M_J}, and skewness $s_{M_J} = \mu_3/\sigma_{M_J}^3$ of the multiplicity distribution for the γ cascades in the reaction products from bombardments of ^{150}Nd with 163.5 and 172.3 MeV ^{20}Ne ions.

			E_{lab} = 163.5 MeV					E = 172.4 MeV				
Final product	E_γ (keV)	J^π Level	σ_J [a] (mb)	$\langle E_\gamma \rangle$ (MeV)	$\langle M_J \rangle$	σ_{M_J}	s_{M_J}	σ_J [a] (mb)	$\langle E_\gamma \rangle$ (MeV)	$\langle M_J \rangle$	σ_{M_J}	s_{M_J}
^{163}Yb + 7n		$\frac{13}{2}^+$	(30 3)					(20 2)				
	203	$\frac{17}{2}^+$	25 7	1.35	27.8 33			20 2	1.35	32.2 30	11.2 50	−1.8 100
	345	$\frac{21}{2}^+$	34 6	1.21	31.8 56	14.6143	−2.0117					
^{162}Yb + 8n		0^+	(157 4)					(61 6)				
	166	2^+	153 4	1.22	23.5 6	8.418	−1.332	33 4	1.22	27.9 30	4.2 218	
	320	4^+	116 22	0.98	29.6 9			58 4	1.06	32.4 18		
	437	6^+	161 6	1.27	23.9 9	4.460	−642	66 6	1.23	29.0 25		
^{161}Yb + 9n		$\frac{13}{2}^+$	(109 11)					(80 5)				
	232	$\frac{17}{2}^+$	109 11	0.88	20.9 7	8.420	1.431	80 5	1.03	23.3 11	6.7 44	−2.4 123
^{160}Yb + 10n		0^+	(71 5)					(108 2)				
	243	2^+	66 4	0.88	12.2 18			109 5	0.88	18.2 8	6.2 28	−2.6 76
	395 [b]	4^+	140 30 [b]	0.61	17.6 6	5.221	−1.568	200 50 [b]	0.88	18.8 9	9.6 20	−0.9 2190
	589	8^+	77 6	0.54	18.6 16			108 9	0.82	20.5 20	7.2 63	−2.4 121
^{159}Er + 7$n\alpha$		$\frac{13}{2}^+$	(77 4)					(35 4)				
	209	$\frac{17}{2}^+$	73 4	1.17	22.4 13	6.652	−3.1156	34 3	1.31	24.5 22	7.2 81	−2.0 207
	350	$\frac{21}{2}^+$	81 7	1.04	25.7 32	12.080	−1.473	36 3	1.22	26.9 26	11.6 74	−1.7 78
^{158}Er + 8$n\alpha$		0^+	(126 11)					(120 7)				
	193	2^+	119 4	0.88	20.5 6	6.026	0.875	115 7	0.97	22.9 7	8.0 21	−0.9 40
	336 [b]	4^+	160 33	0.80	22.9 8	11.320	−2.220	162 16	1.12	20.5 12	8.3 24	−2.1 38
	444	6^+	105 5	0.99	19.5 10			112 6	1.07	22.2 12	8.9 35	−1.0 45
^{157}Er + 9$n\alpha$		$\frac{13}{2}^+$	(58 5)					(99 9)				
	266	$\frac{17}{2}^+$	56 4	0.67	12.1 13	4.841	3.3136	133 16	0.80	15.2 11	6.7 32	−2.2 63
	415	$\frac{21}{2}^+$	60 4	0.53	15.2 18	6.151	−2.5116	88 5	0.83	15.3 12	6.2 35	−2.1 70
^{156}Er + 10$n\alpha$		0^+						(71 6)				
	453	4^+						71 6	0.39	12.9 15	8.6 30	0.4 26

[a] Values obtained for the level yields from measurement of γ rays at 90° corrected for $E2$ angular correlations by multiplying by 1.1.

[b] Probably an unresolved doublet.

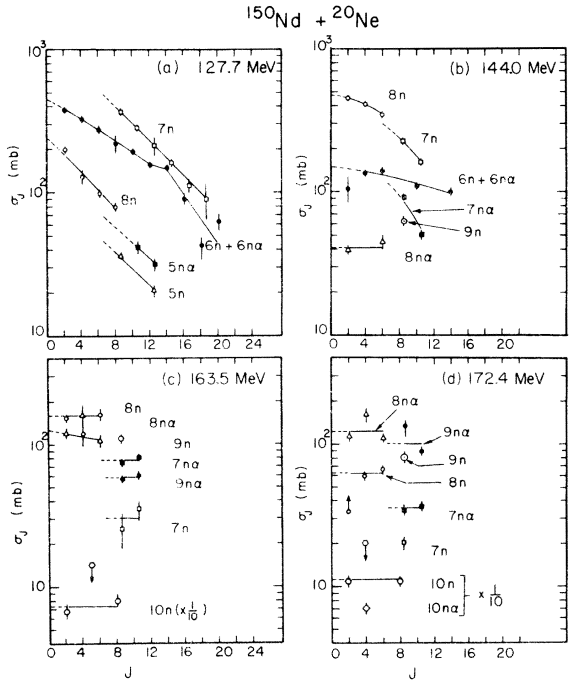

FIG. 2. Measured cross sections σ_J from bombardments of ^{150}Ne with ^{20}Ne at the indicated energies for levels observed in various identified reaction products, as a function of angular momentum J of the gating transition ($J \rightarrow J-2$). The gradual decrease of the side feeding intensity with increasing bombardment energy is apparent.

transitions characteristic of the yrast cascade[5,11-16] via the ground state band of the even $^{160-164}$Yb and $^{156-160}$Er isotopes together with the positive parity bands in the odd-A $^{161-165}$Yb and $^{157-161}$Er isotopes were found to carry about 90% of the γ-ray line strength.

The side feeding pattern of the yrast cascade observed in this work was determined from the measured cross section for each identified level. For the 127.7, 163.5, and 172.4 MeV bombardments, absolute cross sections were determined; these are summarized in column 3 of Table III and columns 3 and 8 of Table IV. The cross sections were derived from the 90° yields in the Ge(Li) detector by multiplying by 1.10 to correct for the effect of stretched $E2$ angular distributions. The γ-ray yields in the Ge(Li) were also corrected for losses due to coincidence summing in the Ge(Li) detector itself. These were taken to a good approximation as $1/(1-\Omega_0 W)^{M-1}$, where Ω_0 is the overall efficiency of the Ge(Li) detector at the average cascade energy $\langle E_\gamma \rangle$, W is the angular correlation function for detecting any two of the γ rays in the cascade in the Ge(Li) detector at 90°, and M is the total multiplicity in the cascade. The corrections amounted to 5–15% for $M = 12-32$. In the case of the 144.0 MeV bombardment only relative cross sections were determined. These were normalized to 1140 mb for all the evaporation residues based on the measured total fusion cross section of Zebelman *et al.*[3] by subtracting the measured fission cross section of 89 and 220 mb (see discussion in Ref. 3). The partial cross sections for each transition are displayed in Figs. 2(a)–2(d) and listed in Tables II and IV. The cross sections listed for the 0^+ ground states in the even products and for the $i_{13/2}$ bandheads in the odd products have been determined by the extrapolation shown in the graphs. At the lower two bombardments considerable side feeding intensity is observed [Figs. 2(a) and 2(b)]. As the bombardment energy is increased the population pattern shifts rapidly toward the high-spin states, as evidenced by the flattening out of the curves in Fig. 2. The similarity of level structure in ^{164}Yb and ^{160}Er interfered with the precise determination of the cross sections and multiplicities for the $6n$ and $6n\alpha$ channels. The cross sections plotted in Fig. 2 refer to the sum for ^{164}Yb + ^{160}Er; the cross section for the $6n\alpha$ product ^{160}Er was estimated from the low-fold spectra to be about one-half of that for the $6n$ product ^{164}Yb.

The excitation functions are shown in Figs. 3(a) and 3(b). At the lower two bombardment energies the dominant products are from the (^{20}Ne, xn) reactions with $x = 6$, 7, and 8. At the higher energies a large fraction of the observed products involves the emission of an α particle. A careful examination of the very complex spectra obtained

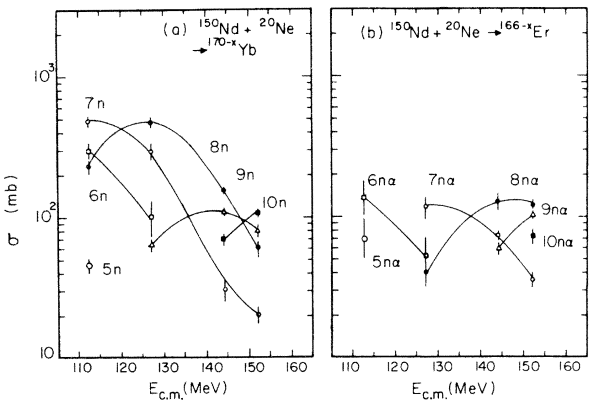

FIG. 3. Excitation functions of the products formed in the bombardment of ^{150}Nd with ^{20}Ne. The cross sections are based on γ-ray intensities deexciting the ground state bands in the even-A products extrapolated to the 0^+ ground state and the $i_{13/2}$ band in the odd-A products extrapolated to the $\frac{13}{2}^+$ J value as indicated in Fig. 2. It is seen that at higher energies the α-particle-emitting reactions carry a larger fraction of the cross section.

at the highest energy revealed products associated with the (^{20}Ne,xnp) and possible (^{20}Ne,$xn2\alpha$) reactions. The high level density of some of the (^{20}Ne,xnp) products made it very difficult to determine their cross sections and multiplicities. Preliminary examination of the particle evaporation spectra from further studies[9] of the ^{150}Nd + ^{20}Ne reactions at 175 MeV revealed appreciable cross section for proton-emitting reactions.

At the highest energy appreciable cross section for events leading to fission is expected.[3] This perhaps is responsible for the large increase of the structureless background observed in the γ-ray spectra at the high energies.

D. Multiplicities

Since some side feeding was observed in the 127.7 and 144.0 MeV products, the results from the first of these energies were analyzed by the two methods outlined in Secs. II A and II B. In the simpler version (Sec. II A) the incoming multiplicity $\langle M_{in} \rangle$ and its second and third moments were extracted for the cascades entering a state by gating on a transition deexciting that state. The resulting multiplicities were found to decrease by unity as one moves up by one level in the ground state band. From these, the overall multiplicities were obtained as $\langle M_J \rangle = \langle M_{in} \rangle + \frac{1}{2}(J_{\text{level}} - J_g)$, where J_g is the angular momentum where the cascade terminates. For the odd-mass products transitions from the deexcitation of the $\frac{13}{2}^+$ states were of such low energy that either they fall below the discriminator level or were highly converted and therefore did not contribute to the observed coincidence rates. For the 127.7 MeV data the more detailed analysis (Sec. II B) was employed whenever possible to extract directly the side feeding multiplicity from the observed data. Within experimental error these results were consistent with the simpler analysis discussed above. In view of the fact that at the highest two energies there was no observed side feeding, these results were only analyzed by the method described in Sec. II A.

The multiplicities are summarized in Tables III and IV. Columns 6, 7, 8, 11, 12, and 13 in Tables III and IV give the total multiplicity $\langle M_J \rangle$, the standard deviation $\sigma_{M_J} = \mu_2^{1/2}$, and the skewness $s_{M_J} = \mu_3/\sigma_{M_{in}}^3$ through the gating transition $J \rightarrow J-2$. Since in this work all cascades below the gating transition involve only stretched $E2$ transitions without branching, σ_{M_J} and s_{M_J} are taken as $\sigma_{M_{in}}$ and $s_{M_{in}}$, respectively. The observed multiplicities $\langle M_J \rangle$ from the 127.7 and 144.0 MeV experiments are illustrated in Figs. 4(a) and 4(b), respectively. In the case of the ^{164}Yb and ^{160}Er products the curves shown represent the average $6n + 6n\alpha$ multiplicities. In view of the fact that the $6n\alpha$ cross section is $\sim \frac{1}{2}$ of that for the $6n$ product, the $6n$ multiplicity should be higher by ~two units. From Figs. 4(a) and 4(b) the constancy of $\langle M_J \rangle$ with J is clearly seen. Most striking, however, is the difference in $\langle M_J \rangle$ between products differing by the number of emitted neutrons, amounting to a decrease in $\langle M_J \rangle$ by about five units for every additional removed neutron. Also, it is interesting to note that the multiplicity $\langle M_J \rangle$ for the $xn\alpha$ products is in general noticeably lower than for the $(x+1)n$ product.

The widths of the multiplicity distributions are seen from Table III to be also independent of J. Furthermore, within the uncertainties for σ_{M_J} there is no significant difference in width for the xn and the $xn\alpha$ products. There is, however, a systematic variation of the J-averaged width σ_M with the number of emitted neutrons at fixed bombardment energy and with bombardment energy for a given product. In Table V the J-averaged $\langle M \rangle$, σ_M, and skewness, s_M, are summarized for each product. In Figs. 5(a)–5(d) σ_M and s_M are plotted vs the number of emitted neutrons. In this case the width and skewness for the xn and $xn\alpha$ products have been averaged together. It is seen that σ_M decreases with increasing x, while the skewness s_M increases with increasing x going from negative to near zero as n changes from 6 to 10.

Figure 6 depicts the variation of $\langle M \rangle$ with bombardment energy for each product. Two reaction channels, namely ^{163}Yb + 7n and ^{162}Yb + 8n, where observed at all four energies and exhibit an almost linear increase with increasing bombardment energy. The near parallel behavior of these curves of $\langle M \rangle$ vs E_{lab} is striking. The $\langle M \rangle$

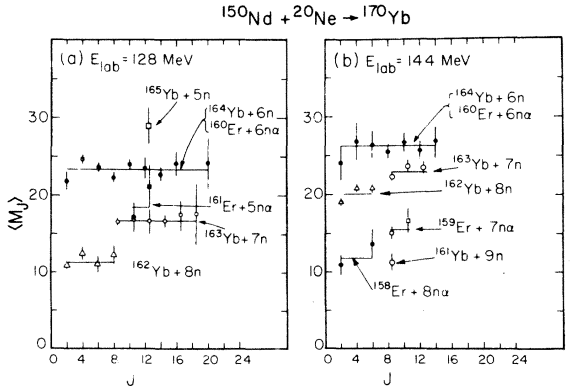

FIG. 4. Average multiplicity $\langle M_J \rangle$ as a function of J of the gating transition ($J \rightarrow J-2$) in the various reaction products formed in ^{150}Nd bombardments by ^{20}Ne at 127.7 and 144.0 MeV. The multiplicities are seen to be independent of J even when considerable side feeding is present (Fig. 2).

TABLE V. Values of the multiplicity $\langle M\rangle$, multiplicity width σ_M, and skewness $s_M=\mu_3/\sigma_M^3$ obtained as weighted averages of the corresponding values for levels with different J^π values in the various identified evaporation residues following reactions of ^{150}Nd with ^{20}Ne at the indicated bombardment energies. The underlined numbers are explained in Table I.

E_{lab}	Identified evaporation residue										
	^{165}Yb	^{164}Yb+^{160}Er	^{163}Yb	^{162}Yb	^{161}Yb	^{160}Yb	^{161}Er	^{159}Er	^{158}Er	^{157}Er	^{156}Er
127.7 MeV											
$\langle M\rangle$	27.1 23	23.2 2	16.60 23	11.2 3			18.2 16				
σ_M		6.87 80	5.8 7	5.9 8							
s_M		−1.25 152	−0.54 126	0.09 131							
144.0 MeV											
$\langle M\rangle$		26.1 4	22.7 4	20.1 2	11.2 12			15.4 8	11.7 11		
σ_M		7.2 31	6.9 14	6.0 11	3.7 45			7.7 19	3.1 46		
s_M		−2.1 67	−3.1 38	−1.1 27				−1.0 26			
163.5 MeV											
$\langle M\rangle$			28.8 28	25.3 4	20.9 7	17.2 5		22.9 12	21.0 4	13.1 11	
σ_M			14.6 143	7.5 16	8.4 20	5.2 21		8.2 43	9.3 16	5.3 32	
s_M			−2.0 117	−1.2 43	1.4 31	−1.5 68		−1.7 66	−2.0 19	−0.1 88	
172.4 MeV											
$\langle M\rangle$			32.2 30	30.8 15	23.3 11	18.6 6		25.5 17	22.3 15	15.2 8	12.9 15
σ_M			11.2 50		6.7 44	8.4 16		9.6 55	8.2 14	6.5 24	8.6 30
s_M			−1.8 100		−2.4 123	−1.1 18		−1.7 73	−1.4 23	−2.2 47	0.4 26

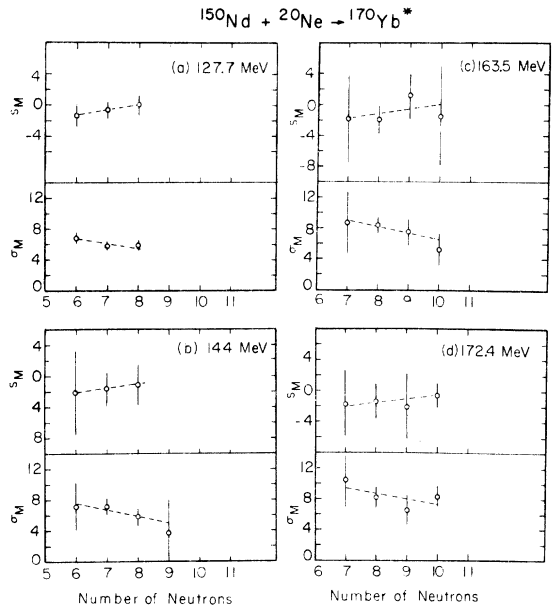

FIG. 5. Width σ_M and skewness s_M of the multiplicity distribution averaged over J in the various reaction products as a function of the number of emitted neutrons x from reactions induced by ^{20}Ne on ^{150}Nd at the indicated bombardment energies. It is seen that for a given energy the width σ_M decreases with increasing x while the skewness s_M approaches zero with increasing x (more symmetric distributions at high x). The width σ_M at given x is seen to increase with bombardment energy.

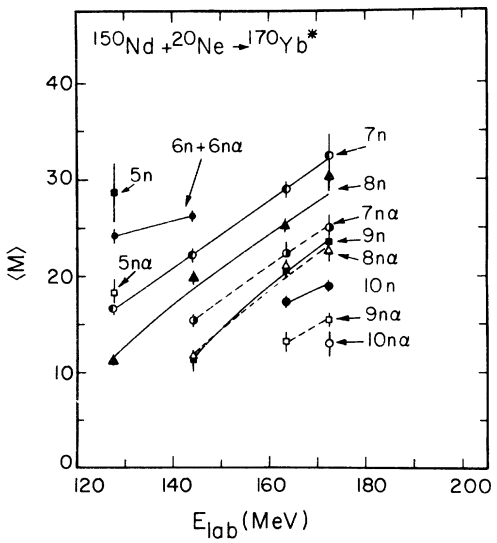

FIG. 6. Average multiplicity $\langle M\rangle$ of the γ cascades in the various reaction products formed in bombardments of ^{150}Nd by ^{20}Ne as a function of bombardment energy. It is seen that $\langle M\rangle$ increases with energy and that the highest $\langle M\rangle$ values are associated with the products emitting the fewest neutrons at a given bombardment energy.

TABLE VI. Total fusion and evaporation residue cross sections, $\bar{l}_{ER}$, $\bar{l}_{crit}$, $\bar{l}_{crit}$(Bass), $\bar{J}_{xn}$, $\bar{J}_{xn\alpha}$, $\bar{J}_{xn+xn\alpha}$, and $\bar{l}_{\alpha}$ values deduced in this work at the four bombardment energies used. The average number of neutrons $\bar{x}$ and $\bar{x}_{\alpha}$ emitted in the xn and $xn\alpha$ reactions are also given.

	E_{lab} (MeV)			
	127.7	144.0	163.5	172.4
$E_{c.m.}$ (MeV)	112.7	127.1	144.3	152.1
σ_{fus} (mb)		(1230 ± 220) [a]		
σ_{ER} (mb)	1265 ± 190 [b]	1140 ± 220 [a]		
$\sigma_{xn+xn\alpha}$ (mb)	1265 ± 190 [b]		625 ± 93 [b]	594 ± 89 [b]
$\bar{l}_{ER}$	41.2 ± 3.0	41.4 ± 4.0		
$\bar{l}_{crit}$		43.1 ± 3.9		
$\bar{l}_{crit}$(Bass) [c]	38.6	43.4	48.6	50.8
$\bar{J}_{xn}$	30.7 ± 1.0	36.9 ± 1.4	39.9 ± 1.0	42.0 ± 1.2
$\bar{J}_{xn\alpha}$	29.4 ± 3.0	27.9 ± 2.4	32.7 ± 1.0	31.5 ± 0.8
$\bar{J}_{xn+xn\alpha}$	30.5 ± 1.0	35.6 ± 1.2	36.8 ± 0.8	36.2 ± 0.8
$\bar{x}$	6.9	7.5	8.6	9.0
$\bar{x}_{\alpha}$	5.7	7.0	8.2	8.6
$\bar{l}_{\alpha}$	2.7 ± 3.2	9.6 ± 2.8	7.6 ± 1.4	10.9 ± 1.5

[a] From Ref. 3.
[b] From this work.
[c] Calculated from the Bass model of Ref. 18.

values for the $xn\alpha$ products are considerably lower than for the xn or even the $(x+1)n$ products. It is also seen that the spacing between the xn and $(x+1)n$ lines is uneven, indicating a decreased $\langle M \rangle$ for the odd-A products because the last detected γ ray in the cascade populates the $\frac{13}{2}^+$ level, compared to the 0^+ level for the even products.

From the results presented thus far it is evident that the distributions in M correspond to cascades with large average number of γ rays (11–32) and are quite broad, having $\sigma_M \sim 30$–60% of $\langle M \rangle$. These large widths indicate that although the various channels involve γ cascades which have distinctly different $\langle M \rangle$, the cascade lengths for the formation of the various products have distributions that overlap considerably.

V. ANGULAR MOMENTUM BALANCE

In complex fusion reactions such as $(^{20}\mathrm{Ne}, xny\gamma)$ or $(^{20}\mathrm{Ne}, xn\alpha y\gamma)$ it is not easy to delineate the angular momentum balance. In previous work the orbital angular momentum transferred was deduced in a simplistic way from the measured total fusion cross section. The moments of the multiplicity distribution measured in this work for each evaporation residue allow one to approach the problem of angular momentum balance from the final steps of this multistage process. Before this can be done, however, the average angular momentum dissipated per γ ray, f, must be known. In earlier work[7] f was deduced from comparison of multiplicity results with fusion cross sections. In such comparisons, however, the angular momentum removed by the evaporated particles and by fission should not be ignored.

In Table VI we have summarized the parameters pertinent to the angular momentum balance. The $xn + xn\alpha$ cross section of 1265 ± 175 mb for the 127.7 MeV experiment is believed to account well for the total cross section in the evaporated residues. For the 144 MeV experiment the value of (1140 ± 220) mb was obtained from Zebelman *et al.*[3] by subtracting the fission cross section and one standard deviation from their reported total fusion cross section of 1450 ± 220 mb which they consider[3] to be too high. For the highest two energies $\sigma_{xn+xn\alpha}$ does not represent the total evaporation residue cross section since the $(^{20}\mathrm{Ne}, xnp\gamma)$, $(^{20}\mathrm{Ne}, xn2\alpha\gamma)$ and other reactions are significant.[9] The values of $\bar{l}_{ER}$ shown in Table VI, derived from σ_{ER} for the lowest two energies are in good agreement with the predictions of the Bass model.[17]

The dissipation of angular momentum by the γ cascades is better understood by defining as the "statistical transitions" those that proceed primarily toward the yrast line from the equiprobability line for neutron and γ-ray emission. The remaining transitions, called the yrast cascades, include the stretched quadrupole and dipole transitions which proceed primarily along or parallel to the yrast line. Statistical model calculations for the mass-60 region[18-24] indicate that the statistical cascades have $\overline{\Delta J}_{st} \sim 0.2$, while the yrast cascades are dominated by streched $E2$ transitions even in a nondeformed nucleus like ^{61}Cu. In this work we assume that $\overline{\Delta J}_{st} = 0$ and that the average angular momentum removed per

γ ray in the yrast cascade is $2\hbar$. Recently Newton *et al.*[22] have reported the observation of six yrast and six "statistical" γ rays in the cascades from the ^{148,150}Sm(^{16}O, $4n$) reactions. Independently Trautmann *et al.*[23] have reported multiplicities for statistical γ rays in the range 2–6. Simon *et al.*[24] assumed four statistical γ rays on the average in the reaction ^{126}Te(^{40}Ar, $4n$) ^{162}Yb.

From the present measurements of $\bar{l}_{ER}$ at 127.7 and 144.0 MeV and of the multiplicities a relationship can be established between the average angular momentum $\overline{\Delta J_n/\bar{x}}$ removed by each evaporated neutron, the number M_s of statistical transitions and the average angular momentum f_y removed per γ ray in the yrast cascade. The average angular momentum $\bar{J}_{xn}$ for all the xn reaction products can be calculated via

$$\bar{J}_{xn} = \frac{\sum_i \sigma_i [(\langle M \rangle - M_s) f_y + J_g]_i}{\sum_i \sigma_i} , \qquad (13)$$

where σ_i is the cross section for the ith product, and J_g gives the angular momentum of the state where the cascade terminates. In what follows the value of 2 for f_y will be used. This assumption is consistent with the findings of Banaschik *et al.*[25] and of Simon *et al.*,[24] who concluded from angular distribution measurements in the γ continuum that most of the nonstatistical transitions are stretched $E2$ in character. The average angular momentum removed per neutron, given by

$$\overline{\Delta J_n/\bar{x}} \equiv \frac{\bar{l}_{ER} - \bar{J}_{xn}}{\bar{x}} , \qquad (14)$$

takes the values of 0 for $M_s = 0$, 0.5 ± 0.3 for $M_s = 2$, and 1.1 ± 0.3 for $M_s = 4$ for 127.7 and 144.0 MeV. Statistical model calculations[18-21] indicate that about one unit of angular momentum may be expected to be removed per evaporated neutron on the average, implying $M_s = 4$. This is consistent with the experimental results from similar reactions at lower excitation energy.[22-25] The average angular momenta $\bar{J}_{xn}$, $\bar{J}_{xn\alpha}$, and $\bar{J}_{xn+xn\alpha}$ for the xn, $xn\alpha$, and total ($xn + xn\alpha$) evaporation residues calculated from Eq. (13) with $M_s = 4$ and $f_y = 2$ are summarized in lines 8, 9, and 10 in Table VI. Using these $\bar{J}_{xn}$ and $\bar{J}_{xn\alpha}$ values one can calculate the orbital angular momentum carried by the emitted α particles in the present reactions as follows:

$$\bar{l}_\alpha = (\bar{J}_{xn} - \bar{J}_{xn\alpha}) + (\bar{x} - \bar{x}_\alpha) \frac{\overline{\Delta J_n}}{\bar{x}} , \qquad (15)$$

where $\bar{x}$ and $\bar{x}_\alpha$ are the average number of neutrons emitted in the xn reactions and the $xn\alpha$ reactions (lines 11 and 12 of Table VI). The second term in the above expression corrects for the additional angular momentum removed by the somewhat larger average number of neutrons $\bar{x}$ associated with the xn reactions compared with $\bar{x}_\alpha$ for the $xn\alpha$ reactions. The results are given in the last line of Table VI. In this analysis $M_s = 4$ was used for all bombardment energies. This is, perhaps, a reasonable assumption in view of the fact that if this treatment is applied to the data of Ref. 7, the energy dependence of the parameter f (Fig. 7 in Ref. 7) is essentially removed.[26]

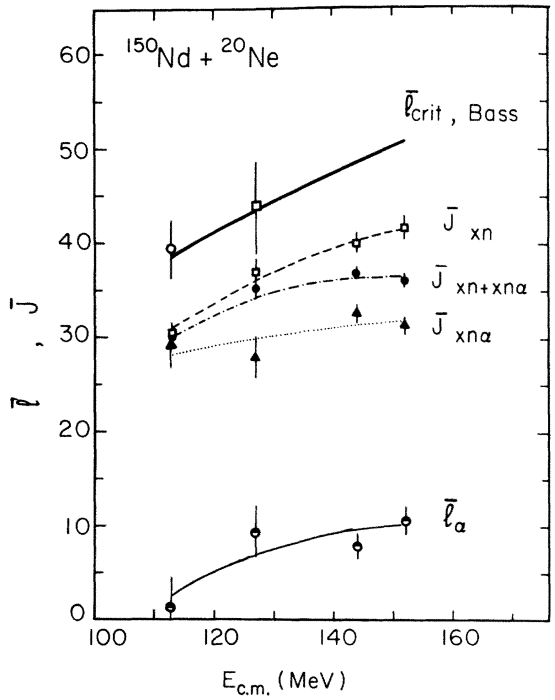

FIG. 7. Average angular momenta $\bar{J}_{xn}$, $\bar{J}_{xn\alpha}$, and $\bar{J}_{xn+xn\alpha}$ deduced from multiplicity measurements as a function of the center-of-mass energy (see text) in bombardments of ^{150}Nd by ^{20}Ne. The lines drawn through the data points (dashed, dashed-dotted, and dotted lines) are to guide the eye. The solid line is the predicted $\bar{l}_{crit}$ value from the Bass model. The open circle is the $\bar{l}_{ER}$ value and the square is the $\bar{l}_{crit}$ value based on the fusion cross section of Ref. 3. The half-closed circles give the deduced average orbital momentum $\bar{l}_\alpha$ removed by the α particles.

The results of Table VI are displayed in Fig. 7. The solid line is the $\bar{l}_{crit}$ prediction of the Bass model.[17] The value of $\bar{l}_{ER}$ for the 127.7 MeV data from this work is in good agreement with the Bass model. At the highest two bombardment energies comparisons with the Bass model are not possible because only part of the important reaction products are observed and the fission cross sections are not known. From Fig. 7 it is seen that $\bar{J}_{xn\alpha}$ increases with bombardment energy but with distinctly different slope than $\bar{l}_{crit}$ (Bass). However, $\bar{J}_{xn+xn\alpha}$ is observed to level off at $\simeq$36. It is also interesting to note that $\bar{l}_\alpha$ (thin

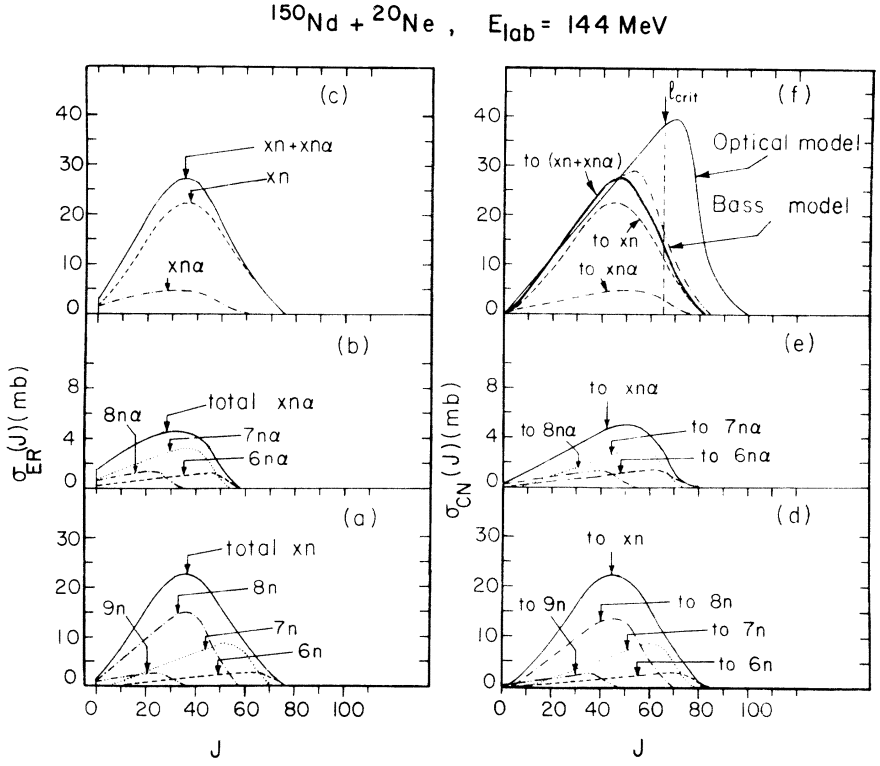

FIG. 8. Angular momentum distributions in the evaporation residues prior to γ decay as deduced from multiplicity measurements for the (^{20}Ne,xn) and (^{20}Ne,$xn\alpha$) reactions on ^{150}Nd at 144 MeV are shown in (a) and (b), respectively. The J distributions in all the xn, $xn\alpha$, and ($xn+xn\alpha$) products are shown in (c) as dashed, dashed-dotted, and solid lines, respectively. The deduced J distributions in the compound nuclei that lead to the various xn and $xn\alpha$ products are shown in (d) and (e). The dashed and dotted-dashed curves in (f) show the J distributions that lead to all the xn and $xn\alpha$ products; these are also shown in solid lines in (d) and (e). The thick solid line in (f) gives the J distribution that leads to all xn and $xn\alpha$ products. The vertical arrows in all cases give the $\bar{J}$ value for each product. The thin solid line in (f) gives the optical model prediction for the total reaction cross section for each partial wave with $l=J$. The vertical dashed line depicts the sharp cutoff value for l_{crit} from the Bass model that leads to fusing collisions. The double-dot dashed curve gives the Bass model prediction modified by assuming a dropoff in the high-l transmission coefficients equal to that given by the optical model.

solid line) appears to increase with bombardment energy, as shown clearly by the difference between the dashed and dotted lines. The value of $\bar{l}_\alpha$ depends only weakly on the assumed value of M_s.

VI. ANGULAR MOMENTUM DISTRIBUTION IN THE EVAPORATION RESIDUES

The moments of the multiplicity distribution were converted to the moments of the distribution in J for each identified product nucleus as follows: $\bar{J}=(\langle M\rangle - M_s)f_y + J_g$, $\sigma_J = f_y\sigma_M$, and $s_J = s_M$ with $f_y = 2$ and $M_s = 4$, as discussed in Sec. V. With only three moments it is not possible to construct a unique distribution but the gross features are well determined since the known moments are the ones of lowest order.

For most of the products the skewness s_M was found negative and approaching zero for the reactions with the higher numbers of emitted neutrons (Fig. 5). Since the errors of s_M were large, the value of $s_M = s_J = -0.57$, corresponding to a triangular distribution[7] increasing with J, will be used. The triangular distributions constructed in this way were rounded at the top to a 90% to 10% width of about 15 units of angular momentum in order to avoid an unrealistic sawtooth summed distribution. In Figs. 8(a) and 8(b) the distributions in J for the (^{20}Ne,xn) and (^{20}Ne,$xn\alpha$) products formed in the 144 MeV bombardments are shown. In both cases the heaviest lines correspond to the sum. Two important observations can be made from these figures. First, there is a strong overlap of the J distributions for neighboring isotopes. Second, states with J in excess of 50 are strongly populated in the $7n$ and $6n$ reaction products. The $xn\alpha$ products have J distributions which are shifted to lower J value, as

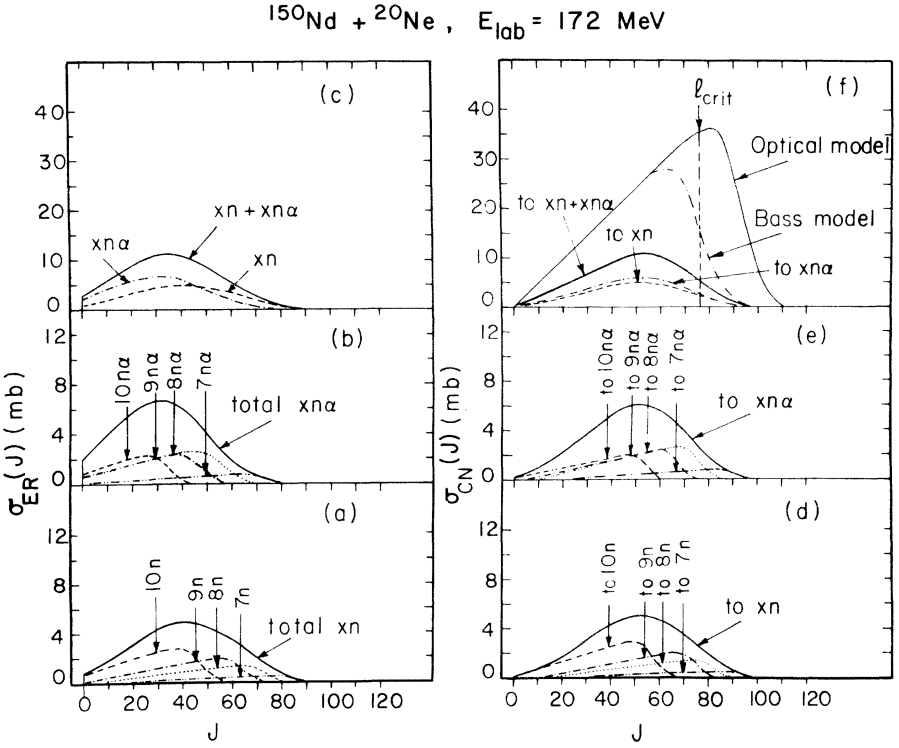

FIG. 9. The curves shown from the 172 MeV data have the same meaning as in Fig. 8.

expected since α particles can carry off much angular momentum. In Fig. 8(c) the total J distributions for the xn, $xn\alpha$, and $xn+xn\alpha$ products are displayed.

The distributions shown in Figs. 8(a)–8(c) correspond to the evaporation residues after particle emission but prior to γ decay. (Of course, γ emission may occur before particle emission but its effect is expected to be negligible.) By introducing information on the angular momentum carried off by particle emission it is possible to construct the J distributions in the initial compound nucleus. For this purpose, the width and skewness are taken to be the same, $\sigma_J = \sigma_M$ and $s_J = s_M$, but the average values are adjusted for the angular momentum removed by the emitted particles. Thus the value of

$$\overline{J}_{c\to x} = (\langle M\rangle - M_s)f_y + x\frac{\overline{\Delta J}_n}{\overline{x}} + J_g ,$$

with $f_y = 2$, is used for each (^{20}Ne,xn) product. For the (^{20}Ne,$xn\alpha$) products the $\overline{J}_{c\to x}$ value is increased by $\overline{l}_\alpha$ taken from Fig. 7. The results are displayed in Figs. 8(d) and 8(e). Similar overlap between adjacent products is observed as in Figs. 8(a) and 8(b). The total J distribution in the initial compound nucleus that leads to both the xn and $xn\alpha$ evaporation residues is now displayed as the heaviest line in Fig. 8(f). The other full line shows the σ_i distribution from the optical model for collisions that represent the total reaction cross section. The optical model parameters employed[27] were $V_0 = 41.8$ MeV, $W = 16.4$ MeV (volume absorption only), $R = 10.115$ fm for the real and the imaginary radii, and 0.49 fm for the real and imaginary diffuseness parameters. The Bass model prediction[17] gives a sharp cutoff l_{crit} of 65. The dashed-double dot line in Fig. 8(f) gives the distribution from the Bass model in which the sharp cut-off distribution has been modified by using transmission coefficients that give a more realistic dropoff in the distribution, identical to that found with the optical model at higher l values. Such a modified Bass model accounts well for the J distribution deduced from the present measurements. The fission cross section observed[3] at 144 MeV is accounted for by decay from compound nuclei formed with J values in excess of ~50, above which the probability for fission becomes large.[3]

A similar analysis was carried out for the other bombardment energies. In all cases the angular momentum distributions exhibit strong overlap for exit channels over several adjacent neutron numbers. The J distributions for 127.7 MeV are similar to those of Fig. 8 with the cut-off J valu

and the widths σ_J being somewhat smaller. The Bass model accounts well for these distributions. For the highest two energies of 164.5 and 172.4 MeV, however, considerable differences are observed. In Fig. 9 the J distributions from the 172.4 MeV data are presented. The J values in the evaporation residues in Figs. 9(a) and 9(b) are about 10 units higher than those of Figs. 8(a) and 8(b) with some of the $7n$ products reaching $J \simeq 85$. In Fig. 9(c) the total xn and $xn\alpha$ J distributions are compared. The most probable J in the $xn\alpha$ products is about 10 units lower than in the xn residual nuclei. It is interesting to note that although the total xn and $xn\alpha$ distributions are now similar [Fig. 9(f)], a pronounced difference exists between the distributions leading to the highest cross section $10n$ product [Fig. 9(d)] and the $8n\alpha$ product [Fig. 9(e)]. The latter reaches J values that are ~20 units higher than the $10n$ product. In fact, this effect persists in the evaporation residues [Figs. 9(a) and 9(b)], where it is seen that the $8n\alpha$ product reaches J values of ~55, whereas the $10n$ product reaches J values of ~45. It is clear from Fig. 9(f) that considerable cross section from both low and high J values has not been observed. The pxn and $xn2\alpha$ reactions, not included in this analysis, could account for the missing low and medium J populations. Most of the missing high J population probably leads to fission.

From the deduced J distributions one may derive information about the regions of an E^* vs J diagram where the various decay modes, such as neutron, α particle, or γ emission dominate. For this purpose one observes from Fig. 3 that the maxima of the xn and $(x-1)n\alpha$ excitation functions occur at approximately the same bombardment energy. At 144 MeV the (^{20}Ne, $8n$) cross section is about 4 times that for (^{20}Ne, $7n\alpha$), but at 172.4 MeV the $10n$ and $9n\alpha$ products have nearly equal cross sections. For the latter case the J distributions [Figs. 9(a) and 9(b)] are very similar, indicating that the $9n\alpha$ must originate from considerably larger spin values (since the α particle carries away on the average an angular momentum of ~$10\hbar$) [Figs. 9(d) and 9(e)]. If the α particle is emitted at an early stage, i.e., before most of the neutrons, then the subsequent deexcitation path should appear as an xn reaction occurring at lower energy and angular momentum. In such a case the widths σ_M in the $xn\alpha$ product should be smaller than the corresponding xn product with the same x. However, the σ_M values from the xn and $xn\alpha$ reactions at the same bombardment energy and the same x are within error the same. If on the other hand the α particle is emitted at the end of the neutron cascade from a region near the yrast line for large J values where α emission is of comparable strength with γ emission, then the following observations would be naturally explained. Namely, (a) the widths σ_M in the xn and $xn\alpha$ products are the same, and (b) the widths in the $xn\alpha$ product are lower than in the $(x+1)n$ product despite the fact that the $xn\alpha$ products originate from distributions extending to higher J values than the $(x+1)n$ in products. Statistical model calculations[28] also indicate the

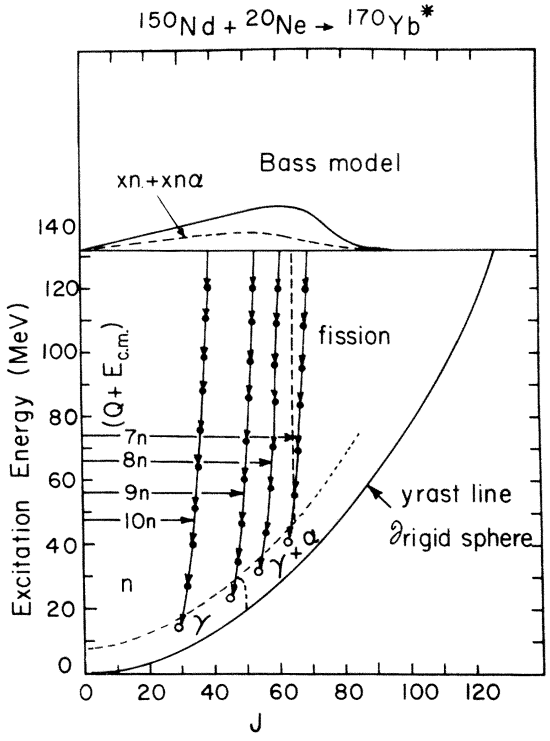

FIG. 10. Schematic diagram for the deexcitation of ^{170}Yb* compound nuclei formed at 132 MeV of excitation in 172.4 MeV ^{20}Ne bombardment of ^{150}Nd. The expected J population in ^{170}Yb from fusing collisions is shown at the top as a solid line according to the Bass model prediction. The dashed line at the top shows the deduced J population that leads to $(xn + xn\alpha)$ reactions. The yrast line, which corresponds to a rigid sphere value for the nuclear moment of inertia for $A = 162$, $r_0 = 1.2$ fm, is a rather schematic superposition of all products; each of them has a different yrast line. The downward cascading arrows depict deexcitation by neutron emission and start from the deduced $\langle J \rangle$ value that leads on the average to products ranging from $7n$ to $10n$. The open circles represent the average position where the neutron cascades terminate (see text). The line defined by these open circles is essentially parallel to the yrast line and indicates that the line of equal neutron and γ-ray emission probability lie somewhat higher (dashed line). The vertical dashed line depicts the J values above which the probability for fission is expected (Ref. 3) to be $\geq 50\%$. At some value of $J \sim 50$ along the yrast line γ and α emission are expected to compete (see text).

existence of a region near the yrast line and above some high J value where α emission is expected to dominate.

It is instructive to discuss the present results with respect to an $E^* - J$ population diagram. In Fig. 10 we show a deexcitation diagram of the $^{20}Ne + ^{150}Nd$ system from the 172.4 MeV bombardment. The yrast line drawn corresponds to that of a rigid sphere and was evaluated for $A = 162$ with $r_0 = 1.2$ fm via $E_{rot} = (\hbar^2/2\mathcal{I}_{rig})J(J+1)$. The open circles have coordinates given by $E^* = \langle T'_\gamma \rangle$ and $J = \bar{J}_i$ for the $10n$, $9n$, $8n$, and $7n$ reactions. It is interesting to note that the partition of the available energy $(E_{c.m.} + Q)$ into $\langle E_n \rangle + \langle T'_\gamma \rangle$ as discussed earlier when combined with the $\bar{J}_i$ values from the multiplicity data defines a line which is essentially parallel to the yrast line. This line for $M_s = 4$ gives an average energy for the statistical γ rays of ~2.1 MeV if the rigid sphere yrast line is assumed. This result is in good agreement with the findings of Trautmann *et al.*,[23] who reported E_{eff} and $\bar{N}_\gamma$ values for the statistical cascades in $(^{16}O, xn)$ reaction leading to $^{157\text{-}162}Yb$ products. Furthermore, the total energy $\langle E_n \rangle$ imparted to neutrons gives average neutron energies of 3.3 and 4.5 MeV for the $10n$ and $7n$ products. This is consistent with the average neutron energy observed in the time-of-flight measurement[9] for this reaction. At the top of Fig. 10 are shown the J distribution from the Bass model for complete fusion and the total $(xn + xn\alpha)$ J distribution as deduced in this work. The neutron cascades shown by arrows are a schematic representation of the deexcitation assuming the same average neutron energy for all steps. This path follows the average population of states in the (E^*, J) diagram. However, these populations overlap strongly and the various decay modes compete for the available channels primarily near the end of the cascade. For J values larger than 65 the results of Zebelman *et al.*[3] indicate a probability for fission larger than 50%. Although a region of high α emission probability near the yrast line may be expected[1] above $J \sim 50$, it is apparent that considerable γ strength persists to high J values since, in addition to arguments given above, the J distribution for the $(^{20}Ne, 7n)$ product extends to $J \sim 85$.

VII. DISCUSSION

The results of this investigation have demonstrated that it is possible to determine the average multiplicities and infer the average angular momentum for many evaporation residues in heavy ion induced reactions for compound nucleus excitation energies as high as ~130 MeV. Furthermore, from measurements of the higher moments of the multiplicity distribution the distributions in J for the various evaporation residues can be deduced. The present findings clearly support the results of Hagemann *et al.*,[7] who find strong overlap in the J distributions in the $^{150}Nd(^{16}O, xn)$ products for $x = 4$ and 5. The concept of "bins" in E^* vs l^2 space in which the various reaction products fall[5] is not substantiated by the present results. In fact, we find that the overlap between the J distributions extends to products differing by three or four neutron numbers (see Figs. 8 and 9).

The present results give no indication for a lower l cutoff, as has been suggested for some Kr induced reactions.[29]

The dependence of $\langle M \rangle$ and therefore $\bar{J}$ for a particular product on bombardment energy was found to be strong (Fig. 6). However, it appears that for a given xn product at the maximum of its excitation function $\langle M \rangle$ is ~18. The same multiplicity is observed for the $xn\alpha$ products at the maximum of their excitation functions even though their maxima are shifted upward in energy relative to the xn products with the same neutron number x.

The total multiplicity at the high energies used in this work was found independent of the J of the gating transition even when side feeding was observed (127.7 and 144 MeV data). A similar result was reported by Hagemann *et al.*[7] for their highest bombardment energy (see Fig. 3 in Ref. 7) and for cascades[30] following the reaction of $^{64}Ni(^{16}O, \alpha 2n)$ at 67 and 81 MeV.

The results from the bombardments at 165 and 172 MeV suggest that the α-particle emission occurs after neutron evaporation.

The excellent cooperation of the staffs of the Oak Ridge isochronous cyclotron and of the Washington University cyclotron is appreciated. We are grateful to Mr. J. T. Hood and the Washington University cyclotron machine shop for the design and construction of the apparatus. One of us (JHB) wishes to thank the Research Corporation for support.

‡Work supported in part by the U.S. Energy Research and Development Administration.

†Deceased 3 June 1976.

*Operated by Union Carbide Corporation for the U. S. Energy Research and Development Administration.

[1] A. Fleury and J. M. Alexander, Annu. Rev. Nucl. Sci.

24, 279 (1974).
[2]M. N. Namboodiri, E. T. Chulick, J. B. Natowitz, and R. A. Kenefick, Phys. Rev. C 11, 401 (1975).
[3]A. M. Zebelman, L. Kowalski, J. Miller, K. Beg, Y. Eyal, G. Jaffe, A. Kandil, and D. Logan, Phys. Rev. C 10, 200 (1974).
[4]N.-H. Lu, D. Logan, J. M. Miller, T. W. Debiak, L. Kowalski, Phys. Rev. C 13, 1496 (1976).
[5]P. O. Tjøm, F. S. Stephens, R. M. Diamond, J. de Boer, and W. E. Meyerhof, Phys. Rev. Lett. 33, 593 (1974).
[6]E. der Mateosian, O. C. Kistner, and A. W. Sunyar, Phys. Rev. Lett. 33, 596 (1974).
[7]G. B. Hagemann, R. Broda, B. Herskind, M. Ishihara, S. Ogaza, and H. Ryde, Nucl. Phys. A245, 166 (1975); and private communication.
[8]D. G. Sarantites, J. H. Barker, and R. Lovett (unpublished).
[9]D. G. Sarantites, L. Westerberg, J. H. Barker, M. L. Halbert, D. C. Hensley, R. A. Dayras, and N. R. Johnson (unpublished).
[10]J. M. Alexander and J. B. Natowitz, Phys. Rev. 188, 1842 (1969).
[11]L. L. Riedinger, D. C. Hensley, P. H. Stelson, N. R. Johnson, G. B. Hagemann, R. L. Robinson, E. Eichler, R. O. Sayer, and G. J. Smith, Oak Ridge National Laboratory Report No. ORNL-4937, 1973 (unpublished).
[12]A. Buyrn, Nucl. Data 11, 327 (1974); 17, 94 (1976).
[13]J. K. Tuli, Nucl. Data 9, 273 (1973); 12, 245, 477 (1974); 13, 493 (1974).
[14]T. W. Burrows, Nucl. Data 18, 553 (1976).
[15]H. Buescher, W. F. Davidson, R. M. Lieder, and C. Mayer-Böricke, Jülich Annual Report KFA, 1973 (unpublished).
[16]H. Buescher, W. F. Davidson, R. M. Lieder, A. Neskakis, and C. Mayer-Böricke, Nucl. Phys. A249, 379 (1975).
[17]R. Bass, Phys. Lett. 47B, 139 (1973); Nucl. Phys. A231, 45 (1974).
[18]D. G. Sarantites and B. D. Pate, Nucl. Phys. A93, 545 (1967).
[19]D. G. Sarantites, Nucl. Phys. A93, 576 (1967).
[20]D. G. Sarantites and E. J. Hoffman, Nucl. Phys. A180, 177 (1972).
[21]J. H. Barker and D. G. Sarantites, Phys. Rev. C 9, 607 (1974).
[22]J. O. Newton, J. C. Lisle, G. D. Dracoulis, J. R. Leigh, and D. C. Weisser, Phys. Rev. Lett. 34, 99 (1975).
[23]W. Trautmann, D. Proetel, O. Häusser, W. Hering, and F. Riess, Phys. Rev. Lett. 35, 1694 (1975).
[24]R. S. Simon, M. V. Banaschik, P. Colombani, D. P. Soroka, F. S. Stephens, and R. M. Diamond, Phys. Rev. Lett. 36, 359 (1976).
[25]M. V. Banaschik, R. S. Simon, P. Colombani, D. P. Soroka, F. S. Stephens, and R. M. Diamond, Phys. Rev. Lett. 34, 892 (1975).
[26]B. Herskind, in Macroscopic Features of Heavy-Ion Collisions, Argonne National Laboratory Report No. ANL/PHY-76-2, 1976 (unpublished).
[27]N.-H. Lu (private communication); E. H. Auerbach and C. E. Porter, in *Proceedings of the Third Conference on Reactions Between Complex Nuclei, Asilomar, 1963,* edited by A. Ghiorso, R. M. Diamond, and H. E. Conzett (Univ. of California Press, Berkeley, 1963).
[28]J. Gilat, E. R. Jones, III, and J. M. Alexander, Phys. Rev. 7, 1973 (1973).
[29]H. Gauvin, Y. LeBeyec, M. Lefort, and R. L. Hahn, Phys. Rev. C 10, 722 (1974).
[30]M. L. Halbert, P. O. Tjøm, I. Espe, G. B. Hagemann, B. Herskind, M. Neiman, and H. Oeschler, Nucl. Phys. A259, 496 (1976).